JCTC Journal of Chemical Theory and Computation

Article

pubs.acs.org/JCTC

Reaction Dynamics of ATP Hydrolysis in Actin Determined by *ab Initio* Molecular Dynamics Simulations

Holly Freedman,*[,†,§] Teodoro Laino,[‡] and Alessandro Curioni[‡]

[†]CCMAR, FCT, University of Algarve, Campus de Gambelas, Faro, Portugal

[‡]IBM Research—Zurich, Rüschlikon, Switzerland

Supporting Information

ABSTRACT: Energy released by the hydrolysis of the high-energy phosphate bond of nucleoside triphosphate (NTP) cofactors is the driving force behind most biological processes. To understand how this energy is used to induce differences in protein structure and function, we examine the transfer of vibrational energy into the nucleotide-bound actin active site immediately after reaction activation. To this end, we perform Born−Oppenheimer molecular dynamics simulations of the active site at the level of density functional theory (DFT) starting at the calculated transition state (TS) structure. Similarly to the mechanism determined in many nucleotide-bound protein systems, the O_s-P_γ bond is first elongated. Then, nucleophilic attack of the lytic water on P_γ occurs. Subsequently, protons are transferred in a cycle formed by water molecules, a protein residue, Asp154, and the γ-phosphate group, resulting in the formation of $H_2PO_4^-$. To investigate the possible creation of excited vibrational states in the products, power spectra of bond-length autocorrelation functions for relevant bonds within the active site are compared for simulations that start at the TS, at reactants, and at reaction end products. The hydroxyl bond formed in the final proton transfer to the phosphate molecule is observed to exhibit relatively high kinetic energies and large oscillations during reaction. It is also likely that some of the energy released by the reaction is captured by the low-energy stretching vibrations of the phosphoryl bonds of orthophosphate, which oscillate with large amplitudes in nonequilibrium simulations of end products.

INTRODUCTION

The catabolic processes of cells result in the synthesis of ATP, which binds to key proteins involved in performing cellular work and is hydrolyzed to ADP to release most of the energy needed to drive biological processes. Several computational studies of ATP hydrolysis in different protein environments exist, in which likely reaction pathways have been found by determining a series of minimum energy structures as a function of collective variables representing the reaction coordinates,[1] by scanning the potential energy surface,[2−6] or by determining this surface as a function of collective variables in the metadynamics approach.[7] Little is known, however, about how the energy transfer takes place, and in what form the energy which is used to perform work by the protein system is initially released from this exothermic reaction. *Ab initio* molecular dynamics (AIMD) methods can be used to accurately model chemical reactions and to shed light onto the chemical details of ATP hydrolysis by following the dynamics of the protein/nucleotide system immediately after reaction activation.

We focus on ATP hydrolysis in the protein actin, which is the component protein of one of the dynamic components of the cytoskeleton and plays an important role in many cellular functions including cellular adhesion, cellular motility, and cytokinesis. In the presence of ATP, globular (G) monomeric actin polymerizes to form filamentous (F) actin. The actin filament forms a double-stranded helix, i.e., a pair of steep right-handed helices intertwined around one another; alternatively, it can be viewed as one left-handed helix.[8] The dynamics of F-actin relies upon its ability to hydrolyze ATP,[9] first forming ADP-Pi actin and then releasing phosphate to form ADP actin, which exhibits altered physical properties, including decreased persistence length[10] and increased binding to depolymerization proteins.[11]

Actin is a 375 residue protein with dimensions of 67 by 40 by 37 Å and consists of two domains, a small domain, farther from the filament axis in F-actin, and a larger domain, at a smaller radius from the axis (see Figure 1a).[8] In the figure, the "barbed" end at which polymerization occurs at a higher rate points downward, and the "pointed" end points upward. The two major domains in turn are each composed of two subdomains (SDs): 1 (bottom, left in Figure 1a) and 2 (top, left) comprise the outer domain and 3 (bottom, right) and 4 (top, right) comprise the inner domain. The nucleotide-binding site (Figure1b) is located in a cleft between subdomains 1 and 3. The two residues Glu137[12,13] and His161[12] are believed to be directly involved in catalysis based on structural and mutational studies. His161 belongs to the P2 loop (residues 154−161), one of several loops making up the active site. The P1 loop (residues 11−18) forms another part of the active site and contains Lys18, which is important for stabilizing the β-phosphate group during hydrolysis,[12] and Ser14, whose side chain is thought to rotate following the release of the cleaved phosphate group, which leads to a reorientation of another loop making up part of the active site, namely the sensor loop (residues 71−77).[14] This rearrangement has in turn been linked to the ordering of the Dnase-I binding loop (D-loop, residues 40−48), which is unstructured in ATP actin, into a helical structure.[14,15] The active site also contains a metal

Received: April 26, 2012

   dx.doi.org/10.1021/ct3003282 | *J. Chem. Theory Comput.* XXXX, XXX, XXX−XXX

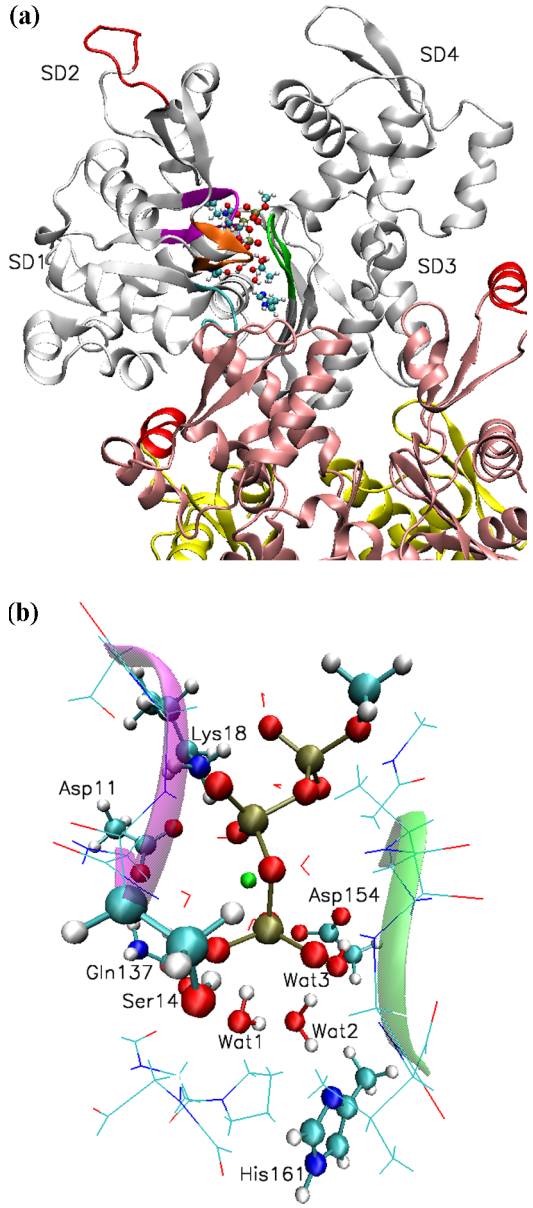

Figure 1. (a) Illustration of actin created from the 1YAG[12] PDB structure (white). The P1 loop is shown in purple, the P2 loop in green, the sensor loop in orange, the proline-rich loop in cyan, and the DB loop in red. The bound nucleotide is shown in stick representation. Two additional actin units (yellow and pink) are depicted where they would be seen in the actin filament. (b) The nucleotide-binding site modeled in this work, oriented in a similar way to that in part a. P1 and P2 loops are shown in cartoon, colored as in part a.

binding site, which is occupied by Mg^{2+} *in vivo*.[8] The Mg^{2+} ion takes on a bidentate conformation, coordinated by nonbridging β- and γ-phosphoryl O atoms of ATP, and four water molecules. Asp residues 11 and 154 on the opposite loops P1 and P2, respectively, help to stabilize two of these coordinating water molecules each.[12]

The actin/ATP system was the focus of a study by Akola and Jones,[1] who used density functional theory (DFT) to determine the most likely reaction pathway based on four calculated paths. In their work, the energetically least costly hydrolysis was found to be a dissociative reaction, meaning that cleavage of the high energy phosphate bond occurs first and, subsequently, the phosphate group is the target of nucleophilic attack by the lytic water, forming ADP and HPO_4^{2-} as end products. On the other hand, it was also found that in the lowest energy product state, the cleaved phosphate group has the form $H_2PO_4^-$.[1]

Regarding the energy transfer, McClare[16] and later Davydov,[17,18] suggested that specific vibrational modes are exploited in the conversion of the chemical energy provided by ATP hydrolysis into work done by the nucleotide-bound protein system.[19,20] Indeed, once this energy has become thermalized, i.e., spread among all available degrees of freedom, very little energy is available to contribute to any specific pathway corresponding to mechanical work. The energy released by ATP hydrolysis (about 8−12 kcal/mol) is of the right magnitude to excite either two quanta of energy corresponding to the amide I vibration, which is mainly a stretch of the C═O group belonging to a peptide bond, or to create an excitation of the main chain NH stretch. Thus, these modes have been predicted to possibly be involved in the mechanism of force generation.[17,18,21−24] According to this proposal, the quantum excitation couples to conformational changes in a protein α-helix, allowing work to be done by the protein system (see ref 25 for a recent review article).

The present study uses a cluster of atoms representing the nucleotide binding site from the 1YAG crystal structure, which was obtained for G-actin in complex with the stabilizing protein gelsolin.[12] Because of the flexibility of the actin filament, actin has not been crystallized in its filamentous form.[26] However, models of F-actin have been created on the basis of X-ray fiber diffraction studies[27−29] and cryo-electron microscopic imaging,[30] which have suggested several structural differences between F- and G-actin. Of particular interest is the cause for the higher rate of ATP hydrolysis in F-actin ($0.3\ s^{-1}$)[31] than that in G-actin, where hydrolysis occurs about 40 000 times more slowly.[32] One theory, based upon the structures of Oda et al.[27] obtained from X-ray fiber diffraction, holds that the main difference is related to a change in the position of Gln137,[26,27,33] whose side chain has been suggested to possibly rotate to bring its amide side chain group into closer contact with ATP and the water molecules involved in catalysis.[34] However, the study by Oda et al.[27] did not include water and stated that it was impossible to deduce details of the reaction mechanism from the diffraction study. Moreover, the structure of F-actin determined by cryo-electron microscopy by Murakami et al.[30] does not show the suggested major shift in the position of Gln137 compared with that seen in G-actin. Those authors hypothesized that the requirement for ATP hydrolysis is instead the downward motion of the proline-rich loop (residues 108−112). According to this model, rearrangement of the proline-rich loop occurs in F-actin when the DB loop of the actin monomer added to the growing, or barbed, end of the filament comes into contact with the proline-rich loop of the actin monomer above it in the filament.[30] In any case, the reader should bear in mind that differences may exist between the structure of the actin active site in F-actin and that in G-actin used here.

In this manuscript, we investigate this reaction mechanism by first determining the minimum energy pathway (MEP) using the nudged elastic band (NEB) method, and then using the resulting saddle point (approximating the transition state (TS) structure) as the starting point in AIMD simulations. Our simulations are performed at the DFT level using the CP2K program package.[35] In this way, we obtain a more detailed

dx.doi.org/10.1021/ct3003282 | J. Chem. Theory Comput. XXXX, XXX, XXX−XXX

picture of the reaction mechanism; in particular, we find that the excess proton is relayed toward the γ-phosphate group, where it remains bound in the final product. To find out which vibrational modes are created by the energy released as the system relaxes out of the TS structure toward the hydrolyzed product system, we determine the bond kinetic energies of a set of atoms involved in the reaction. Moreover, the classical amplitudes of vibrational modes are estimated from the Fourier-transformed bond-length autocorrelation functions, averaged over AIMD simulations, and the spectra calculated in this way are compared for reactants, reacting systems, and reaction products.

METHODS

System Setup. In our study, we adopt the same molecular system as that selected by Akola and Jones,[1] which consists of a cluster of 222 atoms forming the ATP binding site in actin and includes a bound methyl triphosphate (MTP^{4-}) molecule, replacing ATP, and a Mg^{2+} ion. Starting with the 1YAG PDB structure,[12] waters and actin residues were selected on the basis of the criterion of being within 5 Å of the MTP, Mg^{2+}, or Wat709, which we refer to as Wat1. This model has a net charge of −3 and contains 10 water molecules and groups of atoms belonging to the following 18 residues, where charges have been indicated in parentheses: Asp11 (−1), Gly13, Ser14, Gly15, Met16, and Lys18 (+1), belonging to the P1 loop; Gly74, belonging to the sensor loop; Ala108 and Pro109, belonging to the proline-rich loop; Gln137; Asp154 (−1), Gly156, Asp157, Gly 158, Val159, and His161, of the P2 loop; Gly 301 and Gly 302; as well as main chain carbonyl groups from His73 and Glu107. Because catalytic residue His161 is believed to form a water-mediated H bond with Wat1,[12] hydrogen atoms added to a second water, which we refer to as Wat2, were oriented in such a way that one of these forms a hydrogen bond with the N_δ atom of His161. As in ref 1, all main chain C and N atoms and side-chain terminating aliphatic carbon atoms were frozen during all calculations.

The active site system was first briefly energy minimized over 1000 steps of steepest descent minimization, followed by 1000 steps of conjugate gradient minimization, using the AMBER9 classical molecular dynamics program[36] with the AMBER03 force field,[37,38] while freezing all protein atoms, Mg^{2+}, and all oxygen atoms. Parameterization of the nucleotide was taken from ref 39. This allowed the positions of the water H atoms to relax.

Quantum Chemical Calculations. All quantum chemical calculations were performed using the CP2K program package,[35] at the DFT level. Kohn−Sham (KS) orbitals were represented in the DZVP-GTH double-ζ valence basis set employing Goedecker−Teter−Hutter (GTH) pseudopotentials[40−42] for treating interactions between core and valence electrons, together with an auxiliary plane wave basis set.[43,44] A density cutoff for the plane wave basis set of 400 Ry was required because of the inclusion of the contribution of semicore electrons of the Mg^{2+} ion. Calculations were accelerated by initially representing all electrons of the Mg^{2+} ion except its valence electrons by a pseudopotential and obtaining coordinates converged with a density cutoff of 300 Ry, which were used as starting positions for minimizations explicitly treating Mg semicore electrons. Direct inversion of iterative subspace (DIIS) with seven history vectors was used as a minimizer during self-consistent field (SCF) iteration. Two nested SCF loops were used: the inner had 30 cycles and the outer had five cycles. At the end of each inner cycle, the SCF was reset and a new preconditioner was built using the last density guess. PBE[45] with a dispersion correction[46,47] was used as the exchange correlation functional. The wavelet method was used to decouple periodic images when solving the Poisson equation,[48,49] and the cell size used was 20 Å cubic. Geometry optimization was performed using the conjugate gradient (CG) method with a 1D line search algorithm using two-point extrapolation.

Two collective variables were chosen for preliminary exploration of the reaction path, following ref 1. The first is the difference between the distance between P_γ and the O atom of Wat1 and its distance to P_β, given by

$$\mathrm{CV}_1(\vec{r}_{P_\gamma}, \vec{r}_{P_\beta}, \vec{r}_{O_{Wat1}}) = |\vec{r}_{P_\gamma} - \vec{r}_{P_\beta}| - |\vec{r}_{P_\gamma} - \vec{r}_{O_{Wat1}}|$$

The second collective variable we use is the coordination number of H atoms with the O atom of Wat1, defined by

$$\mathrm{CV}_2(\{\vec{r}_{H_i}: i = 1, ..., N_H\}, \vec{r}_{O_{Wat1}}) = \sum_{i=1}^{N_H} \frac{1 - (|\vec{r}_{H_i} - \vec{r}_{O_{Wat1}}|/r_0)^{NN}}{1 - (|\vec{r}_{H_i} - \vec{r}_{O_{Wat1}}|/r_0)^{ND}}$$

where N_H is the number of H atoms. Parameters were set to NN = 6, ND = 12, and r_0 = 1.38 Å, which yielded a close match to the coordination defined by the functional form given in ref 1. These collective variables were restrained during geometry optimization to a sequence of values selected to correspond to a dissociative reaction path, such as is plotted in Figure 4 of ref 1. CV_1 is first increased to effectively elongate the P_γ−O_s bond, and afterward nucleophilic attack of Wat1 on P_γ is achieved by increasing CV_2. Force constants for restraints were set equal to 0.1 hartree/Bohr^2 and 0.1 for the distance difference and coordination number, respectively.

A minimum energy path was determined using the nudged elastic band (NEB) method with a series of 16 images describing the reactive path. Fifty steps of improved tangent (IT) NEB[50,51] were performed before switching on the climbing image (CI) algorithm.[52] The images at the end points were first optimized, and then fixed once they had settled into low-energy conformations. The force constant corresponding to the forces applied between images in the direction of the path was set to 0.05 hartree·Bohr^{-2}, and convergence criteria for maximum values of forces and positions were 0.001 hartree·Bohr^{-1} and 0.0002 Bohr, respectively. Coupled steepest descent/DIIS was used as an optimizer with seven vectors in memory. The frame highest in energy corresponds to our transition state structure. We refer to this configuration as a TS in what follows, although it would be more precise to address it in terms of a saddle point, since no further characterization by frequency calculations or mode following methods was done.

Ab initio Langevin dynamics simulations were run at a temperature of 300 K using a collision frequency of 1.0/ps and a time step of 0.1 fs. Eighty AIMD simulations, each 400 fs in length, were performed starting at the calculated TS structure, using different values of the seed of the random force term. Forty-six simulations were performed starting at the reactant configuration, and another 46 at the optimized product configuration (see below), and 46 at the unoptimized product configuration resulting from one of the AIMD reaction trajectories.

Geometry optimization of the structure corresponding to the major product of AIMD simulations was performed using the

dx.doi.org/10.1021/ct3003282 | J. Chem. Theory Comput. XXXX, XXX, XXX−XXX

CG procedure described above. A similar geometry optimization was performed after rotating the $H_2PO_4^{2-}$ molecule about the bond between the P atom and the Mg-chelating O, to form a hydrogen-bond between the proton of $H_2PO_4^{2-}$, which was transferred from Wat3, and the bridging O from the β-phosphate, using the *autosculpt* feature of the Pymol molecular viewing program.[53] Further optimization of each of these two structures was obtained using 400 steps of simulated annealing molecular dynamics carried out from an initial target temperature of 300 K, with an annealing parameter of 0.97 and a time step of 0.5 fs.

Autocorrelation Functions. The bond velocity and bond length autocorrelation functions were determined as[54,55]

$$C_v[t_m] = \frac{1}{M-m}\sum_{n=0}^{M-m-1}(\vec{v}[t_{n+m}]\cdot\vec{v}[t_n]),\ C_l[t_m] = \frac{1}{M-m}\sum_{n=0}^{M-m-1}(l[t_{n+m}] - l_{avg})(l[t_n] - l_{avg})$$

where v is the difference in velocities between bonded atoms, l is the interatomic distance with average value l_{avg}, and $\{t_n: n = 1-M\}$ is the set of discretized time points. Fourier transformation of autocorrelation functions was performed using the FFTW program[56] after zero padding and applying scaling by the Gaussian function $e^{-m^2/2\sigma^2}$ with width $\sigma = M/3.5$.

RESULTS

Minimum Energy Path. We first performed geometry optimizations of a series of structures of the actin/MTP system along a similar reactive path described by the two collective variables, CV_1 and CV_2, as was plotted in Figure 4 of ref 1. Energies corresponding to this dissociative reaction pathway are plotted in Figure S1 of the Supporting Information, along with the values of the two collective variables. The 12 structures from the calculated reaction pathway were used as initial input structures in the determination of the MEP by NEB calculation. In this method, a number of frames describing the reaction path, in this case 16, are separated from each other by the addition of spring forces between adjacent images that act in the direction tangent to the path.[50] The final energies of the frames and the corresponding values of CV_1 and CV_2 are plotted in Figure 2. As may be seen from Figure 2, the activation energy is determined to be 21.4 kcal/mol.

The overall structure of the reaction pathway for dissociative hydrolysis shown in Figure 2 is the same as that determined in ref 1, although there are minimal differences. Unlike in that study in which the path showed two transition states, we find that there is a single transition state between the initial reactants and the end point structure. Because those authors used a computationally demanding simulating annealing procedure, which allowed global relaxation in the configuration space, a barrier height (21.0 kcal/mol)[1] similar to the one determined here by NEB was obtained. On the other, the CG minimization procedure greatly overestimates the energy barrier, as seen from the apparent activation barrier of 34.9 kcal/mol in Figure S1.

Similar to what was concluded in ref 1, the mechanism of hydrolysis may be summarized as follows based on the results of our NEB calculation. Following dissociation of the nucleotide by elongation of the bond between P_γ and the bridging O_s atom, P_γ is the target of nucleophilic attack by Wat1, in which the OH^- group becomes bound to P_γ, and

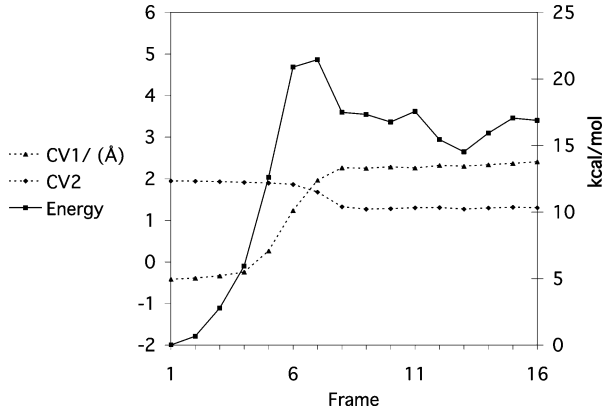

Figure 2. Minimum energy path (MEP) calculated using the NEB method. Collective variables are plotted as a function of the frame number on the left-hand axis, and the energies are plotted on the right-hand axis.

subsequently the excess proton split from Wat1 is shuffled in a Grotthuss-like mechanism first to Wat2, then to a third water Wat3, and finally to a position between Wat3 and Asp154. Figure 3 shows the geometries of the final frames 1, 6, 7, 8, 13, and 14 from the band calculation. Initially, the P_γ atom, the bridging anhydride oxygen atom, O_s, and the O atom of Wat1 are aligned almost linearly. As P_γ draws away from O_s and approaches Wat1, the water molecule rotates so as to form a closer stabilizing link with the amide O of Gln137, and the γ-PO^{3-} group takes on a planar form. In the TS structure (part c), the $P_\gamma-O_{Wat1}$ bond is 1.98-Å-long, and the proton that has been split from Wat1 has transferred to a point about halfway between the O atoms of Wat1 and Wat2. The proton of Wat2 that had been hydrogen-bonded to Wat3 has moved closer to Wat3. The hydrogen bond distance between Wat2 and His161 decreases somewhat as the TS is reached and continues to decrease during the reaction. The two protons involved in this proton wire mechanism have transferred completely to Wat2 and Wat3, in the next step (part d), whereas the proton being transferred to Wat3 remains closely linked to Wat2 so that the two water molecules and the excess proton form a Zundel-like state. In the last steps, Wat3 gradually moves toward the protonated side chain of Asp 154 (parts d–f).

The phosphoryl oxygens that are chelated to Mg^{2+} are shown pointing toward the viewer in Figure 3. These interactions with the Mg^{2+} ion couple the two phosphoryl groups with an O–Mg–O bridge throughout the reaction and stabilize the negative charge added from the reacting hydroxyl group. During reaction, both the $Mg-O_\gamma$ and $Mg-O_\beta$ contacts become closer than in the reactant as the transition state is approached and remain closer as the reaction proceeds from the transition state.

AIMD Simulations. With the TS frame found from the NEB calculations as an initial structure, we performed 80 AIMD simulations, each of a duration of 0.4 ps. Out of these, 27 or 34% returned to the substrate conformation. The main product conformation, in which a proton is transferred from Wat3 to an O_γ atom to form $H_2PO_4^-$, was formed in 46 trajectories. In one trajectory, the system remained in a TS-like conformation throughout the simulation. The remaining six trajectories resulted in the formation of HPO_4^{2-}, with the excess proton, in the final structure, bound in two instances to the terminating amide backbone N of Gly156, in two instances

dx.doi.org/10.1021/ct3003282 | J. Chem. Theory Comput. XXXX, XXX, XXX–XXX

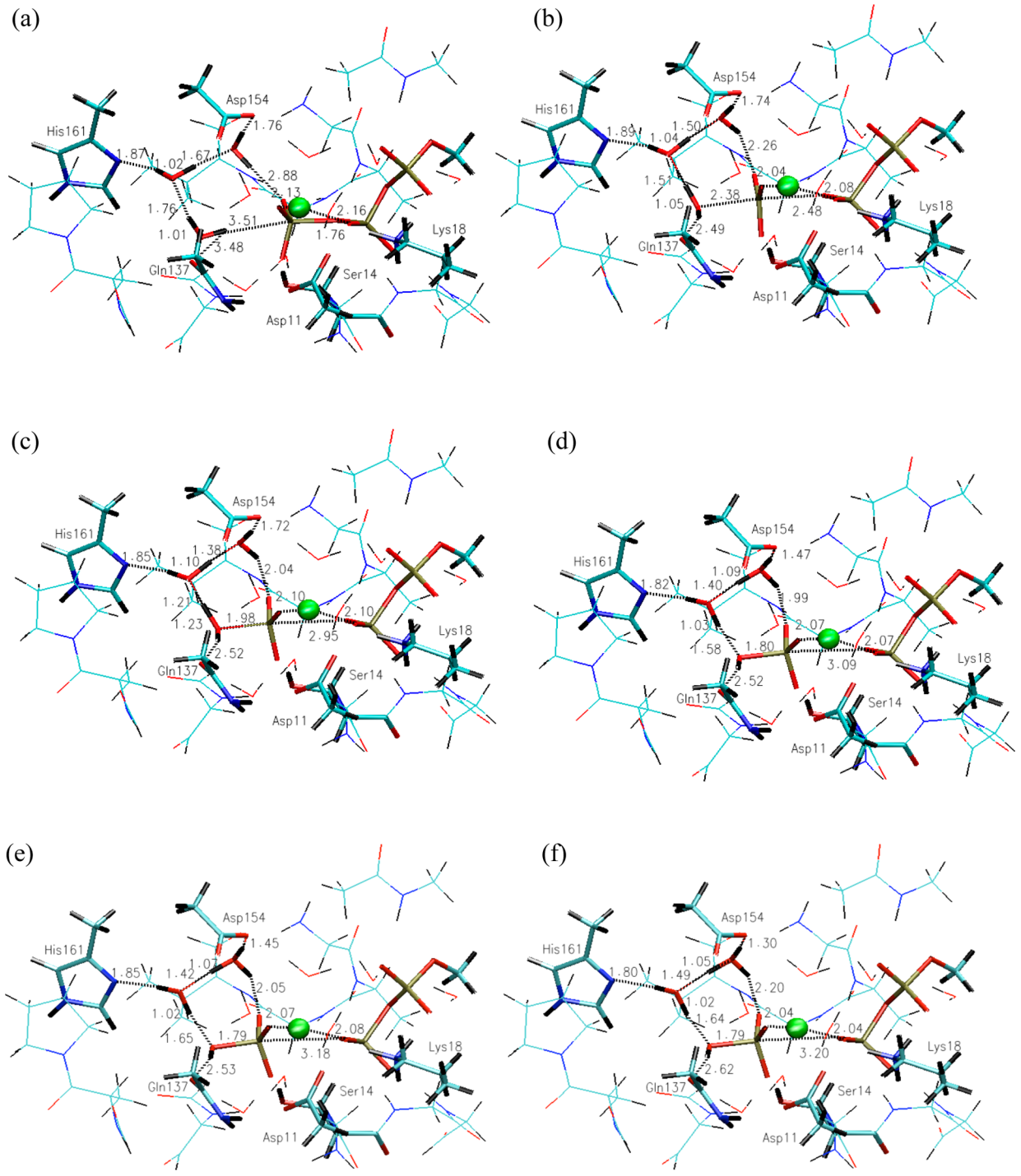

Figure 3. Stick representation of frames (a) 1, (b) 6, (c) 7 (TS), (d) 8, (e) 13, and (f) 14 of the MEP determined in the NEB calculation, with selected distances labeled in Ångstroms.

to the charged side chain of Asp154, and twice hydronium ions were formed from Wat2 and Wat3, respectively.

We performed geometry optimization of the structure corresponding to the major product of the AIMD simulations, for which the energy was found to be 13.0 kcal/mol above that of the optimized reactants. The resulting configuration of the active site is shown in Figure 4. In ref 1, it was concluded that the energetically most favorable final structure is one in which the nonchelating O_γ atom is protonated to form $H_2PO_4^-$, similar to the final structure determined in our AIMD simulations. In that paper, this end product was found to result from another dissociative pathway with a high activation barrier of 28.8 kcal/mol. Moreover, the authors determined a minimum energy structure of this end product in which the phosphate molecule has rotated to form a hydrogen bond with the diphosphate O_β atom, which previously was the bridging O atom in MTP. We therefore rotated the $H_2PO_4^-$ molecule in our product state to form such a hydrogen bond and performed geometry optimization. We found that the energy corresponding to the minimized conformation was 6.7 kcal/mol above that of the reactants. The fact that we did not determine products at a lower energy than that of reactants could be due to our use of

dx.doi.org/10.1021/ct3003282 | J. Chem. Theory Comput. XXXX, XXX, XXX−XXX

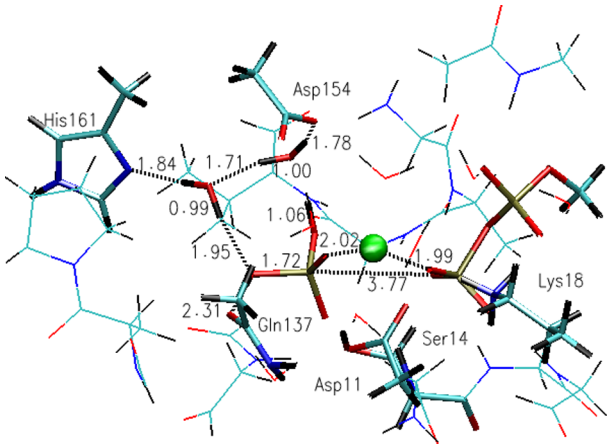

Figure 4. Stick representation of the optimized major end product of AIMD calculations, with selected distances labeled in Ångstroms.

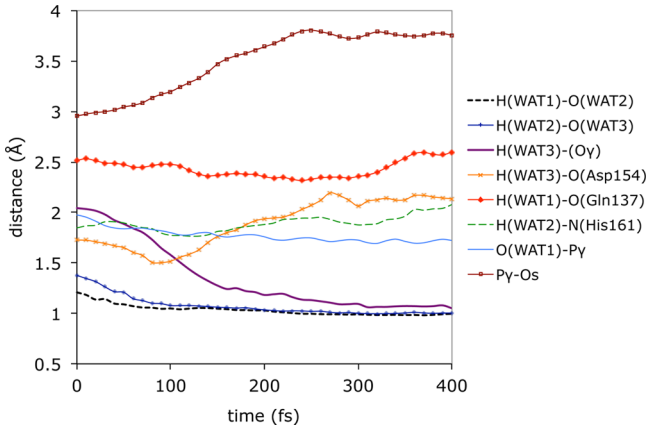

Figure 5. Time evolution of distances averaged over 46 AIMD reaction simulations between protons and water or phosphate O atoms, to which a transfer occurs during reaction, between catalytic protein residues and catalytic waters, between the O atom of Wat1 and P_γ, and between P_γ and O_s.

the nucleotide-binding site from G-actin. Alternatively, the energy may in fact not decrease to a value lower than that of reactants until after the phosphate has left the active site, or there may be another stable configuration of the reagents at a higher energy than both the minimized reactant configuration and the products. In Figure S1, there is a local minimum at the sixth step of the MEP profile, which corresponds to a reactant configuration with a P_γ–O(Wat1) distance of 2.7 Å and an orientation of Wat1 such that its O atom is directed on P_γ, similar to reactant configurations found for other nucleotide-bound protein systems.[3−6,57] While this configuration was found to be unstable within our model, it is important to realize this model's limitations. A more realistic reaction profile might be obtained if full relaxation of the protein binding site and of the solvent are accounted for by using a QM/MM model. Moreover, as in ref 1, we calculate energy differences only, neglecting entropic contributions. Finally, results are sensitive to the accuracy of the pseudopotentials and of the energy functional used; for example, the contribution of the van der Waals correction to the energy functional is quite large, accounting for 4.6 kcal/mol of our calculated energetic difference between reactants and products. In a recent study of ATP hydrolysis in water,[58] a QM/MM model was employed, and entropic contributions were calculated, but the reaction was still predicted to be endothermic, underscoring the difficulty in correctly computing the free energy change for ATP hydrolysis. More accurate knowledge of the magnitude of the free energy change associated with ATP hydrolysis in actin, and of the energetic contribution to this change, will be important for understanding energy transfer since a decrease in energy is needed to account for the ability of vibrational excitations created during hydrolysis to perform work.

In Figure 5, we plot the distances between protons and the O atoms to which these are transferred during the reaction, averaged over the 46 AIMD trajectories producing the major products. Three proton transfers occur as the TS structure is transformed into the final products: one between Wat1 and Wat2, one between Wat2 and Wat3, and the third between Wat3 and an O atom of the γ-phosphate. The first two of these transfers complete within about the first 100 fs of the simulations, as the lengths of the OH bonds formed in the product state decrease from their TS values of 1.21 Å and 1.38 Å, to equal values of 1.00 Å in the product state. The proton transfer from Wat3 to the O_γ atom completes more slowly, within about 300 fs, starting with an H–O_γ distance of 2.04 Å and leading to a final bond distance of 1.05 Å. As was seen in the NEB modeling, there is also a fourth partial proton transfer from Wat3 to a side-chain O atom of Asp154 during part of the reaction. The associated bond, which is 1.72 Å in length at the TS, shortens during the next 90 fs to a length of 1.50 Å and, afterward, as the other proton from Wat3 transfers to the O_γ atom, increases to an average value of 2.14 Å in the product state. In Figure 5, we also show the time evolution of the distance between the side-chain O atom of catalytic residue Gln137 and the H atom of the γ-phosphate belonging to the hydroxyl group derived from Wat1, as well as the hydrogen-bond distance between Wat2 and the catalytic residue His161. The hydrogen bond to Gln137 decreases in length during the first 240 fs of the reaction to a value of 2.32 Å, but hydrogen bonds to both catalytic residues His161 and Gln137 are slightly weaker in the product state than at the TS with lengths of 2.08 Å and 2.60 Å, respectively, to be compared with values of 1.85 Å and 2.52 Å at the TS. We also examined the distances between chelating O atoms and the Mg^{2+} ion, which change little during reaction (not shown).

Comparison to Other Protein Systems. Previously calculated mechanisms of nucleotide hydrolysis in different protein environments exhibit many similarities to the mechanism that our simulations indicate takes place in actin. In the G-protein Ras (p21) studied in ref 4, the excess proton, lost by the lytic water in a dissociative mechanism similar to the one studied here, is passed via a Grotthuss-like mechanism through a second water molecule to the side chain of Gln61 and then back through the second water molecule to the γ-phosphate group to form $H_2PO_4^-$. In fact, the crystal structure of the related protein Rab11 shows that a H atom is most likely shared between the cleaved γ-phosphate and the β-phosphate of the dinucleotide,[4,59] just as ref 1 predicted it to be the case for the optimized end product of ATP hydrolysis in actin. A very similar mechanism to the one in Ras was found in Ras-GAP, the main difference being that the proton transfers involve a cycle formed by only the lytic water, Gln 61, and the γ-phosphate, but again the result is the creation of $H_2PO_4^-$.[4,5] In F1 ATPase, simulations have shown that a proton is transferred from the lytic water to a second water, which is stabilized by the protonated side chain of Glu188, and

dx.doi.org/10.1021/ct3003282 | J. Chem. Theory Comput. XXXX, XXX, XXX–XXX

afterward the second water relays a proton to the γ-phosphate, forming $H_2PO_4^-$.[2] Simulations also predict a dissociative hydrolysis mechanism in myosin, where it was found that the excess proton from the lytic water is transferred through a catalytic water to the side chain of Glu459, in this case creating HPO_4^{2-} as an end product.[3,6]

In contrast, in heat shock protein, Hsc70 ATPase, an associative reaction mechanism is thought to occur whereby there is an initial attack of H^+ from the lytic water on ATP, and afterward the $P_\gamma-O_\beta$ bond is cleaved; in the final reaction steps, OH^- is exchanged from the solvation shell of Mg^{2+} to the solvation shell of K^+, and finally to the P_γ atom.[7]

Kinetic Energy Flow. To investigate the energy flow into the active site, Figure 6 shows the average bond kinetic energies

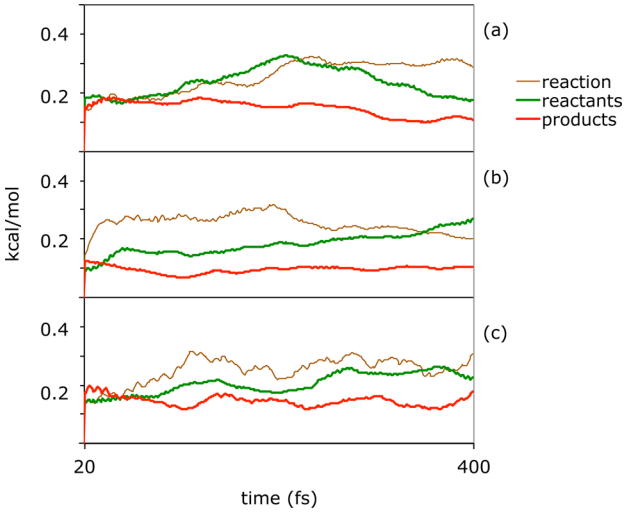

Figure 6. Time evolution of the cumulative average over the last 20 fs of average bond kinetic energies of bonds between (a) H_{Wat1} and O_{Wat2} (reactions and products) or H_{Wat1} and O_{Wat1} (reactants); (b) H_{Wat2} and O_{Wat3} (reactions and products) or H_{Wat2} and O_{Wat2} (reactants); and (c) H_{Wat3} and O_γ (reactions and products) or H_{Wat3} and O_{Wat3} (reactants).

of bonds between protons transferred during the reaction and the O atoms to which these are bonded at the end of the simulation as a function of time. To produce smoother plots, cumulative averaging over the last 20 fs was applied to the average bond kinetic energies. Note that these O atoms are the same in simulations of reactions and products, whereas in simulations of reactants, bonds are within the original Wat1, Wat2, or Wat3 molecules, respectively. In addition, we plot cumulative averages over 20 fs of the average kinetic energies of these protons in Figure S2 of the Supporting Information. Note that in equilibrium simulations, bond kinetic energies would be roughly equal to $kT/2$. The plots show that the three protons involved in transfers in general have higher bond kinetic energies during the reaction than for reactant or product simulations. However, in the plot of the bond kinetic energy of the proton transferred from Wat1 to Wat2 during the reaction, the kinetic energy increases gradually throughout the first 200 fs, during which it differs little between sets of simulations, whereas for the other two protons transferred, bond kinetic energy is relatively high close to the beginning of the reaction trajectories. Unfortunately, the simultaneous thermalization of the system during the simulations complicates the interpretation of the energy data. While the small system size used here makes it difficult to equilibrate the TS prior to simulations, one possible way to remedy this would be to perform QM/MM on a larger system, so that a large part of the system could be properly thermalized before reactions.

The kinetic energies of phosphate PO(H) and P═O bonds and of the $P_\beta O_s$ bond are plotted in Figure 7, and those of the

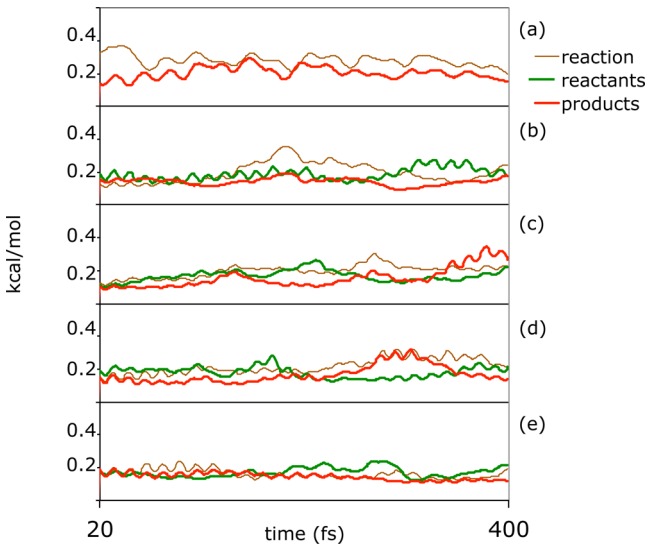

Figure 7. Time evolution of the cumulative average over the last 20 fs of average bond kinetic energies of $P_\gamma O(H)$ bonds involving (a) the O atom derived from the lytic water and (b) the O_γ atom to which a proton is transferred from Wat3 during reaction and of P_γ═O bonds involving (c) the O_γ atom which is hydrogen bonded to Ser14 and (d) the O_γ atom which chelates Mg^{2+}. Average bond kinetic energies of the $P_\beta O_s$ bond are plotted in part e.

O atoms involved are shown in Figure S3. At the beginning of the reaction trajectories, the O atom from the lytic water has a high kinetic energy, as does its bond with P_γ. During the later parts of simulations, the bond kinetic energies of the P═O bond involving the chelating O atom become elevated for reaction and product simulations, as do the bond kinetic energies of the P═O bond involving the nonchelating O atom during product simulations. This indicates that these P═O bonds can easily be excited in the nonequilibrium environment following reaction because of their low vibrational frequencies and high polarities.

To further test whether one or more bonds in the product state may become the receptacle of the energy released by hydrolysis, we determined the power spectra of the bond length and the bond velocity autocorrelation functions of various bonds that are most relevant to the reaction. These functions are closely related to the infrared (IR) absorption spectra, which are given by the Fourier transforms of the dipole autocorrelation functions. Comparisons were made between power spectra calculated for trajectories begun at the TS and those begun at the reaction end product. Only the final 0.1 ps of the 0.4 ps simulations were used in the calculation of the spectra.

We first examined the power spectra of the bonds involving H atoms originally belonging to the three water molecules involved in proton transfers, i.e., Wat1, Wat2, and Wat3 (Figures 8 and 9). Experimentally, liquid water shows a bending mode at 1644 cm^{-1}, a symmetric stretch at 3450 cm^{-1}, and an asymmetrical stretch at about 3600 cm^{-1};[60] the two stretching

dx.doi.org/10.1021/ct3003282 | J. Chem. Theory Comput. XXXX, XXX, XXX−XXX

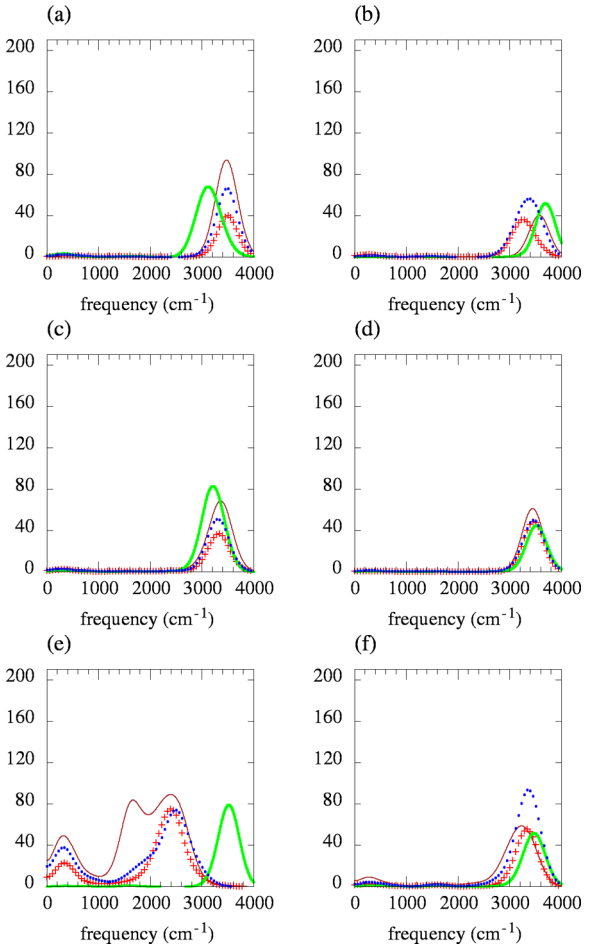

Figure 8. Average power spectra, in arbitrary units, of bond-length autocorrelation functions corresponding to OH bonds involving (a) the H atom transferred from Wat1 to Wat2 during reaction, (b) the H atom of Wat1 belonging to the hydroxyl group transferred to P_γ during reaction, (c) the H atom transferred from Wat2 to Wat3 during reaction, (d) the H atom of Wat2 which is hydrogen bonded to His161, (e) the H atom transferred from Wat3 to P_γ during reaction, and (f) the H atom of Wat3 which is hydrogen bonded to Asp154. (Brown solid lines, reactions; green thick lines, reactants; red crosses, optimized products; blue dotted lines, unoptimized products.)

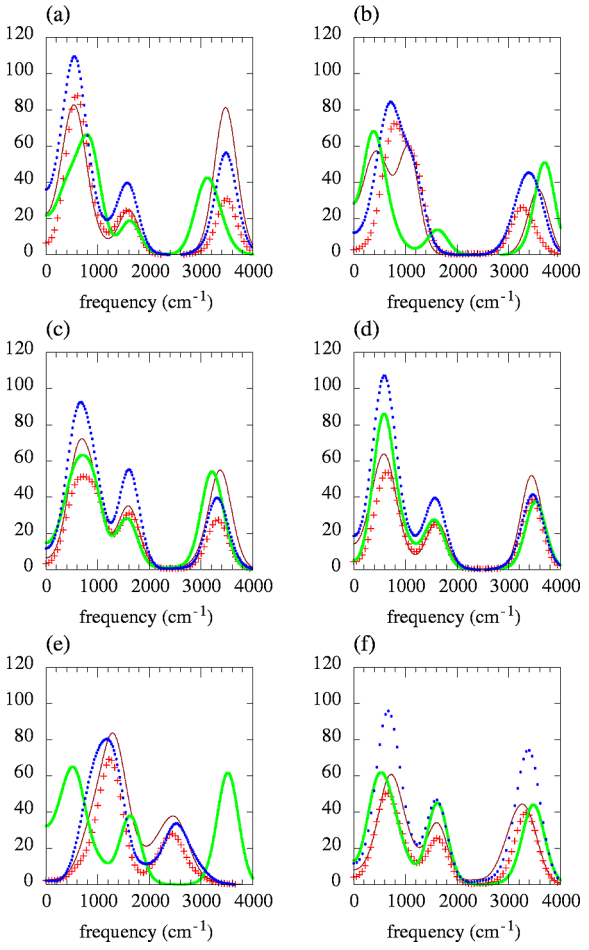

Figure 9. Average power spectra, in arbitrary units, of bond-velocity autocorrelation functions corresponding to the functions plotted in parts a–f of Figure 8. (Brown solid lines, reactions; green thick lines, reactants; red crosses, optimized products; blue dotted lines, unoptimized products.)

vibrations together with an overtone of the bending mode form a broad band centered at 3404 cm^{-1} in the experimental absorption spectrum. The amide I band of proteins in aqueous solution at 1640 cm^{-1} is thought to couple with the bending mode of water,[61] and the stretching vibrations of water are close in frequency to the NH stretch at ~3300 cm^{-1} of the protein main chain. Thus, if a vibrational mode is excited in the protein's aqueous solvation shell, transfer of the excitation to an amide I mode or to an NH stretch in the protein backbone could occur.[62] An increase in vibrational amplitude is seen for the OH stretch at ~3500 cm^{-1} involving the proton transferred from Wat1 to Wat2 during reaction compared with the spectra for the bonds involving the same proton in products (Figure 8a).

In addition, the spectrum of the bond-length autocorrelation function associated with the hydroxyl bond formed by proton transfer from Wat3 to the phosphate molecule shows a very broad band during reaction, with peaks centered at ~1700 cm^{-1} and ~2400 cm^{-1}, spanning a much larger area than the analogous peak centered at ~2400 cm^{-1} corresponding to the isolated product state (Figure 8e). The large amplitude oscillations of this (P_γ)OH bond are strongly influenced by hydrogen bonding to Wat3. Experimentally, the OH stretch of aqueous $H_2PO_4^-$ vibrates at a frequency of 2800–3000 cm^{-1},[63] which is somewhat less than the vibrational frequencies, centered at ~3300–3600 cm^{-1}, observed in our simulations for the phosphate hydroxyl group derived from the lytic water. There is also a second peak in the experimental IR spectrum of aqueous $H_2PO_4^-$ at 2380 cm^{-1} due to the same (P)OH stretch, and it is believed that the existence of the two bands is caused by two potential wells of equal energy between which the proton can quantum mechanically tunnel.[63] Consistently with this theory, the length (1.06 Å) of the (P_γ)OH bond in our optimized AIMD end product for the hydroxyl group stabilized by Wat3 differs greatly from the 0.99 Å bond length of the other (P_γ)OH group, which vibrates at the higher frequency. Examination of individual trajectories and the associated spectra (not shown) that were averaged to calculate the graph in Figure 8e reveals that the peak at ~1700 cm^{-1} results from strong coupling of the proton transferred from Wat3 to the bending mode of the water molecule in a few of the trajectories.

The Fourier-transformed bond-velocity autocorrelation functions (Figure 9) exhibit peaks corresponding not only to the bond stretching modes seen in the spectra of the bond

dx.doi.org/10.1021/ct3003282 | J. Chem. Theory Comput. XXXX, XXX, XXX–XXX

length autocorrelation functions but also to the other vibrational modes. As was seen for bond length autocorrelation functions, higher amplitude peaks centered at ~3500 cm^{-1} and at ~2400 cm^{-1} are seen in parts a and e, respectively, corresponding to stretches of the O(Wat2)H and (P_γ)OH bonds formed during the reaction than in the spectra calculated for products. A comparison of the spectra in the ~1650 cm^{-1} region shows minimal differences between reaction and products, indicating that it is unlikely that an OH bending vibration is excited during the reaction. However, it should be noted that amplitudes of the power spectra of the bond velocity autocorrelation functions can be obscured because of translational or rotational motions (unless a body-centered coordinate system is used, which was not done here).

We also examined the possibility that a phosphoryl bond in the $H_2PO_4^-$ molecule created in the reaction is vibrationally excited. Bands seen in the spectra determined here are centered at values ranging from ~700−900 cm^{-1} for PO(H) stretches and from ~1000−1100 cm^{-1} for P═O stretches (Figure 10 and Figure S4), which are close to the experimental frequencies (878, 947, 1072, 1150 cm^{-1}).[63] Only slight differences can be seen between vibrational amplitudes from reaction, reactants, and optimized products. However, we also performed a set of simulations begun at the unoptimized end point of an AIMD reaction trajectory, and in these trajectories large amplitude oscillations of PO bonds were observed (dotted lines in Figure 10). The bond with the highest amplitude oscillations in these simulations is that between P_γ and the nonchelating O atom, which is hydrogen bonded to Ser14. Because the largest amplitude vibrations of PO bonds are observed in simulations of nonoptimized products rather than in simulations of the reaction, a vibrationally excited state may occur on one of these bonds not as a result of reaction dynamics but rather as the system equilibrates and settles into a lower energy state. As our results indicate, a reduction of the system's free energy compared with that of reactants may not occur during hydrolysis, and it is possible that one or more phosphoryl bonds could be excited at whatever point subsequent to hydrolysis the free energy decreases.

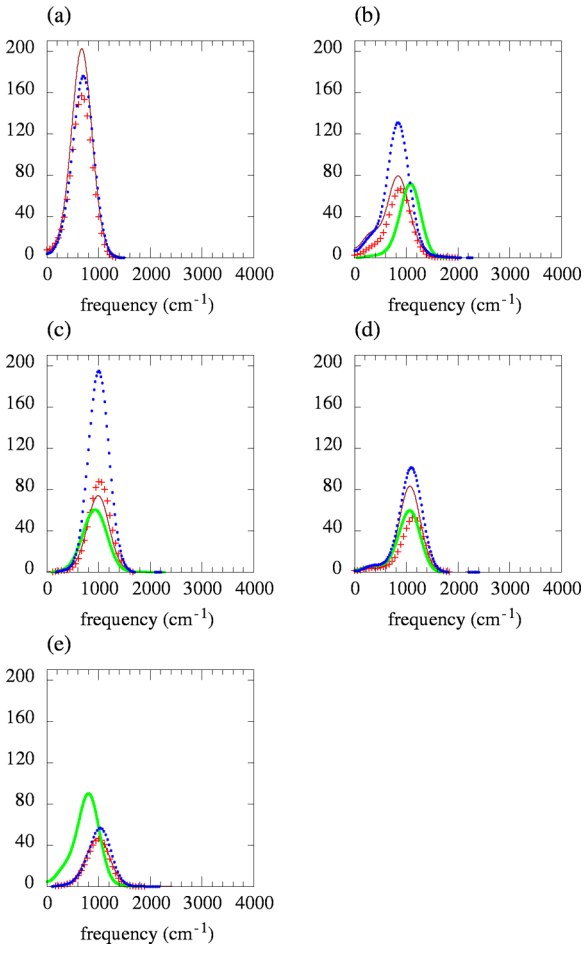

Figure 10. Average power spectra, in arbitrary units, of bond-length autocorrelation functions corresponding to (a) the $P_\gamma O(H)$ bond involving the O atom derived from the lytic water, (b) the $P_\gamma O(H)$ bond involving the O_γ atom to which a proton is transferred from Wat3 during reaction, (c) the P_γ═O bond involving the O_γ atom which is hydrogen bonded to Ser14, (d) the P_γ═O bond involving the O_γ atom which chelates Mg^{2+}, and (e) the $P_\beta O_s$ bond. (Brown solid lines, reactions; green thick lines, reactants; red crosses, optimized products; blue dotted lines, unoptimized products.)

DISCUSSION

We have performed multiple AIMD simulations of the reaction dynamics of a cluster of atoms representing the transition state of actin's active site during nucleotide hydrolysis, by positioning the initial molecular configuration at the TS obtained by NEB calculation and observing the motion of the system as the product state is formed. In 46 out of 52 reactions proceeding to the product side of the transition state, the excess proton cleaved from the lytic water completes a cycle in which it transfers to the γ-phosphate, forming $H_2PO_4^-$ in the product state. As predicted in ref 1, after a proton wire mechanism involving three waters and Asp154, an intermediate is formed in which the excess proton is shared between Asp154 and Wat3. Moreover, consistent with the prediction in ref 1 of the formation of $H_2PO_4^-$ in the lowest energy product state, we find that there is an additional step in which the excess proton is relayed from Wat3 toward the γ-phosphate group, where it is bound in the final product.

The question of which vibrationally excited states are formed following exothermic hydrolysis of ATP within a protein environment is difficult to explore experimentally. By modeling the dynamics of ATP hydrolysis in the actin system, we have identified bonds that may possibly be vibrationally excited during reaction. The proton transferred in the final step to an O_γ atom exhibits higher bond kinetic energies and power spectra with increased amplitudes than it does in the isolated product state. Additionally, the protons transferred to Wat2 and to Wat3 exhibit higher bond kinetic energies during the reaction trajectories than they do in simulations begun at the product state. In a biological system, there is typically tight coupling between the vibrational modes, and thus the vibrational energy released during hydrolysis may be delocalized between the stretches involving the three protons transferred. Because of the large variance in the power spectra for different trajectories, it is also possible that in some instances of ATP hydrolysis, one of the water OH stretching modes is primarily excited, whereas in others, another one or the (P)OH stretch is excited.

Moreover, the P═O bonds formed in the products are highly oscillatory in simulations of nonoptimized product conformations, indicating that one or more of these bonds may also become excited because of environmental perturbations following hydrolysis. The bond between P_γ and the O atom

dx.doi.org/10.1021/ct3003282 | J. Chem. Theory Comput. XXXX, XXX, XXX−XXX

that is hydrogen bonded to Ser14 is roughly parallel to the (P)OH bond that vibrates at ~2400 cm^{-1}, and it is tempting to speculate on the possibility that if a (P)OH vibration with a frequency of ~2400 cm^{-1} is created by the reaction, the interaction with the light-field emitted by a P═O bond stretch may then excite this mode to the alternate higher energy (P)OH stretching mode. Once excited, a vibrational excitation of the (P)OH stretch at ~3300 cm^{-1} may couple with an NH stretch in the protein backbone and transfer through the protein backbone to a site where work is performed, as has been predicted by the Davydov model.[22−24] In this case, ultrashort femtosecond pulses tuned to the lower (P)OH stretch frequency might be used as a means to interfere with interaction with the P═O stretch by the de-excitation or excitation to a higher state of the former mode.

To further explore the question of whether an OH stretching vibration is in the first excited state upon creation of this bond, it will be necessary to use quantum-mechanical methods to study the coupling between quantum vibrations and the dynamics of the surrounding atomic nuclei. A major difference between quantum and classical dynamics is in the larger degree of localization of a quantum vibration.[64−66] This quantum effect has been predicted to allow the very rapid transfer of energy to a specific region in the protein distinguished by distortions in hydrogen bonding structure, where it is needed for protein function.[62]

Structural changes in proteins associated with nucleotide hydrolysis have been probed using time-resolved difference FTIR (Fourier transform infrared) spectra in which nucleotide binding is triggered by the photolysis of caged nucleotides.[67,68] To test experimentally our prediction that (P)OH vibrations may be involved in the energy transfer following ATP hydrolysis, one possible approach would be to compare FTIR spectra obtained in D_2O or D_2O/H_2O mixtures. OD stretching modes in water and in phosphate differ in frequency from the corresponding OH stretching modes.[63] Thus, the coupling between phosphate modes and vibrational modes of the protein backbone, which may be necessary for energy transfer, should be reduced or eliminated in D_2O solvent.

The determination of the initial localization of the vibrational energy immediately following ATP hydrolysis in actin addresses only one aspect of the complex question of how energy transferred from ATP's high-energy phosphate bond is used to perform cellular work. Another important issue is how vibrational energy that may be created is used in protein function, for example whether this energy is used to induce a conformational change in actin which enables the release of the $H_2PO_4^-$ molecule, or whether instead the energy is used to perform the actual conformational changes associated with actin dynamics. The release of phosphate occurs on a very slow time scale, on the order of 10^{-3}/s,[69] whereas excited vibrational modes are thought to become thermalized on a time scale of a few picoseconds.[70,71] However, it has been proposed that, after hydrolysis, the sensor loop changes position, causing the "back door" region[72] consisting of the sensor and proline rich loops to open, so that orthophosphate is released from the nucleotide binding site to an intermediate binding site within the cavity at the interface between the inner and the outer domains.[30] Thus, binding of the $H_2PO_4^-$ molecule at the intermediate site may happen so quickly that it is reasonable to suppose that an excited vibrational state formed during hydrolysis could contribute either to the release of $H_2PO_4^-$ or to related conformational rearrangements occurring in actin.

■ ASSOCIATED CONTENT

Supporting Information

Additional figures (Figures S1, S2, S3, and S4). This material is available free of charge via the Internet at http://pubs.acs.org.

■ AUTHOR INFORMATION

Corresponding Author

*E-mail: hpfreedma@gmail.com.

Present Address

[§]Department of Chemistry, University of Alberta, Edmonton, AB, Canada.

Author Contributions

The manuscript was written through contributions of all authors. All authors have given approval to the final version of the manuscript.

Funding

Grant number SFRH/BPD/41143/2007 to H.F. from the Portuguese Foundation for Science and Technology (FCT).

Notes

The authors declare no competing financial interest.

■ ACKNOWLEDGMENTS

H.F. is grateful for fellowship funding from the Portuguese Foundation for Science and Technology (FCT) under grant number SFRH/BPD/41143/2007. This work was made possible by the facilities and support of the SHARCNET computing network and Compute Canada, and we especially thank Dr. Pawel Pomorski for his assistance. H.F. thanks Prof. Marta Ramos and Prof. Luís Marques for providing a welcome and stimulating environment at the University of Minho, where this work was begun, and Prof. Leonor Cruzeiro for supplying scripts that helped in the data analysis.

■ ABBREVIATIONS

NTP, nucleoside triphosphate; DFT, density functional theory; TS, transition state; ATP, adenosine triphosphate; ADP, adenosine diphosphate; MTP, methyl triphosphate; AIMD, *ab initio* molecular dynamics; F-actin, filamentous actin; G-actin, globular actin; MEP, minimum energy pathway; NEB, nudged elastic band; SCF, self-consistent field; FTIR, Fourier transform infrared

■ REFERENCES

(1) Akola, J.; Jones, R. O. *J. Phys. Chem. B* **2006**, *15*, 8121−8129.
(2) Dittrich, M.; Hayashi, S.; Schulten, K. *Biophys. J.* **2003**, *4*, 2253−2266.
(3) Grigorenko, B. L.; Kaliman, I. A.; Nemukhin, A. V. *J. Mol. Graphics Modell.* **2011**, 1−4.
(4) Grigorenko, B. L.; Nemukhin, A. V.; Shadrina, M. S.; Topol, I. A.; Burt, S. K. *Proteins* **2007**, *2*, 456−466.
(5) Grigorenko, B. L.; Nemukhin, A. V.; Topol, I. A.; Cachau, R. E.; Burt, S. K. *Proteins* **2005**, *3*, 495−503.
(6) Grigorenko, B. L.; Rogov, A. V.; Topol, I. A.; Burt, S. K.; Martinez, H. M.; Nemukhin, A. V. *Proc. Natl. Acad. Sci. U. S. A.* **2007**, *17*, 7057−7061.
(7) Boero, M.; Ikeda, T.; Ito, E.; Terakura, K. *J. Am. Chem. Soc.* **2006**, *51*, 16798−16807.
(8) Chhabra, D.; dos Remedios, C. G. Actin: An overview of its structure and function. In *Actin-binding Proteins and Disease*; dos Remedios, C. G., Chhabra, D., Eds.; Springer: New York, 2008; Vol. 8, pp 1−15.
(9) Belmont, L. D.; Orlova, A.; Drubin, D. G.; Egelman, E. H. *Proc. Natl. Acad. Sci. U. S. A.* **1999**, *1*, 29−34.

(10) Isambert, H.; Venier, P.; Maggs, A. C.; Fattoum, A.; Kassab, R.; Pantaloni, D.; Carlier, M. F. *J. Biol. Chem.* **1995**, *19*, 11437−11444.
(11) Pollard, T. D.; Borisy, G. G. *Cell* **2003**, *4*, 453−465.
(12) Vorobiev, S.; Strokopytov, B.; Drubin, D. G.; Frieden, C.; Ono, S.; Condeelis, J.; Rubenstein, P. A.; Almo, S. C. *Proc. Natl. Acad. Sci. U. S. A.* **2003**, *10*, 5760−5765.
(13) Iwasa, M.; Maeda, K.; Narita, A.; Maeda, Y.; Oda, T. *J. Biol. Chem.* **2008**, *30*, 21045−21053.
(14) Graceffa, P.; Dominguez, R. *J. Biol. Chem.* **2003**, *36*, 34172−34180.
(15) Otterbein, L. R.; Graceffa, P.; Dominguez, R. *Science* **2001**, *5530*, 708−711.
(16) McClare, C. W. *Ann. N.Y. Acad. Sci.* **1974**, 74−97.
(17) Davydov, A. S. *J. Theor. Biol.* **1973**, *3*, 559−569.
(18) Davydov, A. S. *Solitons in Molecular Systems*; D. Reidel Publishing Company: Dordrecht, The Netherlands, 1985.
(19) Scott, A. *Phys. Rep.* **1992**, *1*, 1−67.
(20) Lomdahl, P. S.; Layne, S. P.; Bigio, I. J. *Los Alamos Sci.* **1984**, 1−22.
(21) Careri, G.; Buontempo, U.; Galluzzi, F.; Scott, A. C.; Gratton, E.; Shyamsunder, E. *Phys. Rev. B* **1984**, *8*, 4689−4702.
(22) Scott, A. C.; Bigio, I. J.; Johnston, C. T. *Phys. Rev. B* **1989**, *17*, 12883−12887.
(23) Alexander, D. M.; Krumhansl, J. A. *Phys. Rev. B* **1986**, *10*, 7172−7185.
(24) Alexander, D. M. *Phys. Rev. Lett.* **1985**, *2*, 138−141.
(25) Freedman, H.; Cruzeiro, L. *Curr. Phys. Chem.* **2012**, *1*, 23−32.
(26) Splettstoesser, T.; Holmes, K. C.; Noe, F.; Smith, J. C. *Proteins* **2011**, *7*, 2033−2043.
(27) Oda, T.; Iwasa, M.; Aihara, T.; Maeda, Y.; Narita, A. *Nature* **2009**, *7228*, 441−445.
(28) Oda, T.; Makino, K.; Yamashita, I.; Namba, K.; Maeda, Y. *Results Probl. Cell Differ.* **2001**, 43−58.
(29) Holmes, K. C.; Popp, D.; Gebhard, W.; Kabsch, W. *Nature* **1990**, *6288*, 44−49.
(30) Murakami, K.; Yasunaga, T.; Noguchi, T. Q.; Gomibuchi, Y.; Ngo, K. X.; Uyeda, T. Q.; Wakabayashi, T. *Cell* **2010**, *2*, 275−287.
(31) Blanchoin, L.; Pollard, T. D. *Biochemistry* **2002**, *2*, 597−602.
(32) Rould, M. A.; Wan, Q.; Joel, P. B.; Lowey, S.; Trybus, K. M. *J. Biol. Chem.* **2006**, *42*, 31909−31919.
(33) Pfaendtner, J.; Lyman, E.; Pollard, T. D.; Voth, G. A. *J. Mol. Biol.* **2010**, *2*, 252−263.
(34) Saunders, M. G.; Voth, G. A. *J. Mol. Biol.* **2011**, *1*, 279−291.
(35) The CP2K developers group. http://cp2k.org (accessed August 2012).
(36) Case, D. A.; Darden, T. A.; Cheatham, T. E. I.; Simmerling, C. L.; Wang, J.; Duke, R. E.; Luo, K. M.; Merz, K. M.; Pearlman, D. A.; Crowley, M.; Walker, W.; Zhang, B.; Wang, S.; Hayik, A.; Roitberg, G.; Seabra, K. F.; Wong, F.; Paesani, X.; Wu, S.; Brozell, V.; Tsui, H.; Gohlke, L.; Yang, C.; Tan, J.; Mongan, V.; Hornak, G.; Cui, P.; Beroza, D. H.; Mathews, C.; Schafmeister, C.; Ross, W. S.; Kollman, P. A. *AMBER9*; University of California, San Francisco: San Francisco, CA, 2006.
(37) Duan, Y.; Wu, C.; Chowdhury, S.; Lee, M. C.; Xiong, G.; Zhang, W.; Yang, R.; Cieplak, P.; Luo, R.; Lee, T.; Caldwell, J.; Wang, J.; Kollman, P. *J. Comput. Chem.* **2003**, 1999−2012.
(38) Cornell, W. D.; Cieplak, P.; Bayly, C. I.; Gould, I. R.; Merz., K. M., Jr.; Ferguson, D. M.; Spellmeyer, D. C.; Fox, T.; Caldwell, J. W.; Kollman, P. A. *J. Am. Chem. Soc.* **1995**, *19*, 5179−5197.
(39) Meagher, K. L.; Redman, L. T.; Carlson, H. A. *J. Comput. Chem.* **2003**, *9*, 1016−1025.
(40) Krack, M. *Theor. Chem. Acc.* **2005**, *1*−*3*, 145−152.
(41) Hartwigsen, C.; Goedecker, S.; Hutter, J. *Phys. Rev. B* **1998**, *7*, 3641−3662.
(42) Goedecker, S.; Teter, M.; Hutter, J. *Phys. Rev. B.* **1996**, *3*, 1703−1710.
(43) VandeVondele, J.; Hutter, J. *J. Chem. Phys.* **2007**, *11*, 114105.
(44) VandeVondele, J.; Krack, M.; Mohamed, F.; Parrinello, M.; Chassaing, T.; Hutter, J. *Comput. Phys. Commun.* **2005**, *2*, 103−128.
(45) Perdew, J. P.; Burke, K.; Ernzerhof, M. *Phys. Rev. Lett.* **1996**, *18*, 3865−3868.
(46) Grimme, S. *J. Comput. Chem.* **2006**, *15*, 1787−1799.
(47) Grimme, S.; Antony, J.; Ehrlich, S.; Krieg, H. *J. Chem. Phys.* **2010**, *15*, 154104.
(48) Genovese, L.; Deutsch, T.; Neelov, A.; Goedecker, S.; Beylkin, G. *J. Chem. Phys.* **2006**, *7*, 074105−074109.
(49) Genovese, L.; Deutsch, T.; Goedecker, S. *J. Chem. Phys.* **2007**, *5*, 054704−054709.
(50) Jónsson, H.; Mills, G.; Jacobsen, K. W. Nudged elastic band method for finding minimum energy paths of transitions. In *Classical and Quantum Dynamics in Condensed Phase Simulations*; Berne, B. J., Ciccoti, G., Coker, D. F., Eds.; World Scientific: Singapore, 1998; pp 385−404.
(51) Henkelman, G.; Jónsson, H. *J. Chem. Phys.* **2000**, *22*, 9978−9985.
(52) Henkelman, G.; Uberuaga, B. P. *J. Chem. Phys.* **2000**, *22*, 9901−9904.
(53) Delano, W. L. *The PyMOL Molecular Graphics System*; Schrödinger, Inc.: New York, 2002.
(54) Teatro, T. A. V. Velocity Autocorrelation and Vibrational Spectrum Calculation. http://www.timteatro.net/2010/09/29/velocity-autocorrelation-and-vibrational-spectrum-calculation/ (accessed August 2012).
(55) Kohanoff, J. *Comput. Mater. Sci.* **1994**, *2*, 221−232.
(56) Frigo, M.; Johnson, S. G. *Proc. IEEE* **2005**, *2*, 216−231.
(57) Grigorenko, B. L.; Shadrina, M. S.; Topol, I. A.; Collins, J. R.; Nemukhin, A. V. *Biochim. Biophys. Acta* **2008**, *12*, 1908−1917.
(58) Harrison, C. B.; Schulten, K. *J. Chem. Theory Comput.* **2012**, 2328−2335.
(59) Pasqualato, S.; Cherfils, J. *Structure* **2005**, *4*, 533−540.
(60) Venyaminov, S. Y.; Prendergast, F. G. *Anal. Biochem.* **1997**, *2*, 234−245.
(61) Sieler, G.; Schweitzer-Stenner, R. *J. Am. Chem. Soc.* **1997**, 1720−1726.
(62) Cruzeiro, L. *J. Phys.: Condens. Matter* **2005**, 7833−7844.
(63) Chapman, A. C.; Thirlwell, L. E. *Spectrochim. Acta* **1963**, 937−947.
(64) Cruzeiro-Hansson, L.; Takeno, S. *Phys. Rev. E* **1997**, *1*, 894−906.
(65) Lomdahl, P. S.; Kerr, W. C. *Phys. Rev. Lett.* **1985**, *11*, 1235−1238.
(66) Wang, X.; Brown, D. W.; Lindenberg, K. *Phys. Rev. Lett.* **1989**, *15*, 1796−1799.
(67) von Germar, F.; Galan, A.; Llorca, O.; Carrascosa, J. L.; Valpuesta, J. M.; Mantele, W.; Muga, A. *J. Biol. Chem.* **1999**, *9*, 5508−5513.
(68) Butler, B. C.; Hanchett, R. H.; Rafailov, H.; MacDonald, G. *Biophys. J.* **2002**, *4*, 2198−2210.
(69) Carlier, M. F.; Pantaloni, D. *Biochemistry* **1986**, *24*, 7789−7792.
(70) Hamm, P. *J. Biol. Phys.* **2009**, *1*, 17−30.
(71) Edler, J.; Hamm, P. *J. Chem. Phys.* **2002**, *5*, 2415−2423.
(72) Wriggers, W.; Schulten, K. *Proteins* **1999**, *2*, 262−273.